DOI: 10.1111/tgis.12920

RESEARCH ARTICLE

Transactions in GIS WILEY

Do image resolution and classifier choice impact island biogeographical parameters of terrestrial islands?

Jens Oldeland[1] | Pia Maria Eibes[2] | Severin David Howard Irl[2] | Ute Schmiedel[3]

[1]Eco-Systems, Hamburg, Germany

[2]Biogeography and Biodiversity Lab, Institute of Physical Geography, Goethe-University, Frankfurt am Main, Germany

[3]Biodiversity and Ecology of Plants, Institute of Plant Science and Microbiology, University of Hamburg, Hamburg, Germany

Correspondence
Ute Schmiedel, Universität Hamburg, Institute of Plant Science and Microbiology, Ohnhorsstraße 18, 22609 Hamburg, Germany.
Email: Ute.schmiedel@uni-hamburg.de

Funding information
Bundesministerium für Bildung und Forschung, Grant/Award Number: 01LG1201N—SASSCAL ABC; Deutsche Forschungsgemeinschaft, Grant/Award Number: 404519812

Abstract

Island biogeography provides concepts for conservation management as fragmented habitats are comparable to ocean islands. Remote sensing can help to extract terrestrial habitat islands on the landscape scale. However, little is known about the effects of image resolution and classification algorithms on resulting island size and related parameters. We study the combined effect of three image resolutions (2, 10, and 30 m) and three classification algorithms (Artificial Neural Network, Random Forest, Support Vector Machine) by extracting quartz islands from WorldView-2 imagery using image segmentation. We compared four island parameters (i.e., area, distance, shape index, and perimeter–area ratio between resolutions and classifiers). We found that in all cases, image resolution and classification algorithms had a strong effect. However, image resolution was more important for area and shape. Artificial Neural Network always provided the best performance as a classifier (OA: 0.880, kappa: 0.801, F1: 0.912). Hence, conservation strategies could lead to different results when different pattern extraction strategies are applied. Future studies which aim at extracting terrestrial habitat islands from image datasets should aim for the

highest possible resolution and compare the outcomes of different classifiers to ensure the best possible results.

1 | INTRODUCTION

Isolated special habitats such as forest fragments, rocky outcrops, inselbergs, and remnant grassland patches (Burke, 2002; Itescu, 2019; Matthews, 2021) can be characterized as terrestrial habitat islands embedded in a "sea" of dissimilar matrix habitats (Mendez-Castro et al., 2021; Ottaviani et al., 2020). Due to isolation by distance and specific environmental conditions acting as filters to the species pool, terrestrial habitat islands are often rich in endemic species (Kier et al., 2009). A recent study by Wintle et al. (2019) highlighted the importance of small isolated habitat patches for supporting biodiversity. Consequently, these types of habitats are of particular interest for conservation management and species protection likewise. Island biogeography provides theories that can help to identify areas of high species richness and local endemism, which help conservation managers prioritize areas for conservation management. However, the information on number, size, and distribution of terrestrial habitat islands in an area cannot easily be quantified from the ground. This is particularly difficult in vast and remote areas with reduced access by road. Remote sensing provides the means to extract this information from satellite imagery with high reproducibility, objectivity, and low cost.

Quartz islands, also referred to as quartz fields (Schmiedel & Jürgens, 1999; Van Tonder, Milton, & Cameron, 2014), quartz patches (Curtis, Stirton, & Muasya, 2013), quartz-lag gravel habitat (Ellis & Weis, 2006), or quartz gravel plains (Ellis, Weis, & Gaut, 2006), are edaphic habitat islands in the Succulent Karoo and adjacent biomes of southern Africa, which present a unique, edaphically arid ecosystem surrounded by matrix vegetation on zonal soils (Schmiedel & Jürgens, 1999). These quartz islands have their own vegetation, which differs strongly from the matrix vegetation in terms of structure, composition, and diversity (Eibes et al., 2021; Schmiedel & Jürgens, 1999). Sometimes, sharp boundaries at the scale of a few decimeters between quartz islands and the matrix occur, caused by strong changes in soil pH and electrical conductivity (Schmiedel, Kühne, Twerski, & Oldeland, 2015). Quartz islands are an important habitat for habitat specialists and locally endemic species (Schmiedel, 2002, 2004; Schmiedel & Jürgens, 1999) and conservation areas in South Africa have been implemented to conserve this special habitat type. This is also the case for the Knersvlakte Nature Reserve, our study area. Nevertheless, there is still a considerable lack of detailed spatial information on their distribution at the landscape scale to support conservation management. Many small quartz islands are scattered throughout the landscape, making it difficult to adequately map all quartz islands individually. Indeed, it is still unclear how many quartz islands exist altogether, how much area they cover, and what their spatial configurations are. Remote sensing is a potential tool that could help to create these urgently required maps, potentially discovering hundreds or even thousands of previously unknown habitat islands and aiding conservation management and resource exploitation (esp. mining) by red-flagging ecologically sensitive areas.

Few studies have previously worked on mapping land cover and land use change in the Knersvlakte. Desmet, Cowling, Ellis, and Pressey (2002) provide an example for conservation planning in the Knersvlakte presenting a map based on field work, expert opinions, and herbarium information. Rodríguez-Caballero et al. (2017) used the airborne hyperspectral CASI-sensor to map two types of microbial surface communities, one of them being hypolithic soil crusts on quartz. Although they did not intend to map quartz islands at the landscape scale, they found that quartz islands and surrounding soil types differed strongly in their hyperspectral signatures and that this information could be used to map quartz islands at a larger spatial scale. The best study currently available on mapping quartz islands was performed by De Klerk, Gilbertson, Luck-Vogel, Kemp, and Munch (2016), who wanted to inform practitioners on the best setup to apply to remote sensing to map quartz islands. They compared the suitability of pan-sharpened SPOT-5 (2.5 m) and Landsat 8 (15 m) to map quartz islands on an area of c.

20 × 40 km. Furthermore, they compared 24 different scenarios (e.g., pixel-based vs. object-based classification, two vs. three land cover classes, two different classifiers [Maximum Likelihood vs. Support Vector Machine]), as well as two different image datasets (RGB vs. PCA). They were able to map quartz islands with 99.23% accuracy and a kappa of 0.9 using the object-based image classification and the Maximum Likelihood classifier for the SPOT-5 two-class solution.

Despite the high conservation value of the quartz islands in the Knersvlakte, no map of the quartz island at the landscape scale was made available. Furthermore, new very-high-resolution satellites allow finer spatial resolutions (e.g., the WorldView missions). A higher resolution is also important for testing island biogeography theories on quartz islands, where the size of even small quartz islands within a quartz island archipelago is critical to determine aspects of area, isolation, and insularity (Mendez-Castro et al., 2021). However, for conservation planning and management, where funding is often limited, the use of freely available satellite data can be a relevant criterion. Therefore, Sentinel-2, with a resolution of 10 m, might also be a good candidate for mapping quartz islands given the free-of-charge availability of the image data, higher native resolution (i.e., without pan-sharpening), and more spectral information. Object-based analysis is often the best choice for high-resolution data. Algorithms provided by open-source projects often give equal results to commercial algorithms and are often favored by conservation managers, who typically have constrained budgets (Rocchini et al., 2017). Finally, the combined effects of image resolution and classification algorithms on the variability of island parameters extracted from image segments have not been explored previously in the literature in the context of island biogeography.

With this study, we aim to map quartz islands as edaphic habitat islands at the landscape scale in the Knersvlakte region to support local conservation management in assessing the extent and distribution of endemic-rich quartz islands, as well as providing a baseline for fundamental (island biogeographic) research. We use an extensive ground truth dataset to validate three land cover classes: quartz, matrix, and dense *rivier* (ephemeral river valley) vegetation. After applying open-source object-based image analysis (OBIA) methods, we evaluate three machine learning classifiers applied to three image resolutions and four different image datasets. Finally, we characterize the resulting quartz island dataset by exploring conservation-relevant island characteristics and discuss this pattern in the light of island biogeography.

2 | MATERIALS AND METHODS

2.1 | Study area

The Knersvlakte bioregion is situated in the winter-rainfall-dominated Succulent Karoo Biome (Mucina et al., 2006) in the west of South Africa. It comprises approximately 6300 km^2 (Hoffman, Skowno, Bell, & Mashele, 2018) of a gently undulating plain bordered to the south, east, and north by higher elevated areas and southwest by the Namaqualand Sandveld bioregion (Desmet, 2007). The Knersvlakte is underlain by heterogeneous sediments of the Nama Group, dominated by shale, phyllite, and limestone, and is intruded by numerous quartz veins (Watkeys, 1999) from which the gravel layer of the quartz islands originates (Schmiedel & Jürgens, 1999).

In comparison to other arid areas in South Africa, the Succulent Karoo in general is characterized by mild climate conditions and highly predictable winter rainfall (Desmet, 2007). The Knersvlakte receives an average annual rainfall of 150 mm, with the wet season ranging from May to September (Mucina et al., 2006).

The study was carried out on the farm of Moedverloren (−31.460972°S, 18.449583°E) in the southwestern Knersvlakte, which forms part of the provincial Knersvlakte Nature Reserve (Figure 1). The vegetation of this farm has been classified as unit SKk3 (Knersvlakte Quartz Vygieveld) of the natural vegetation of South Africa (Mucina et al., 2006). The study area is dominated by quartz islands and has not been grazed by domestic livestock for more than 20 years, so that the quartz fields here can be regarded as nearly undisturbed by direct human impact.

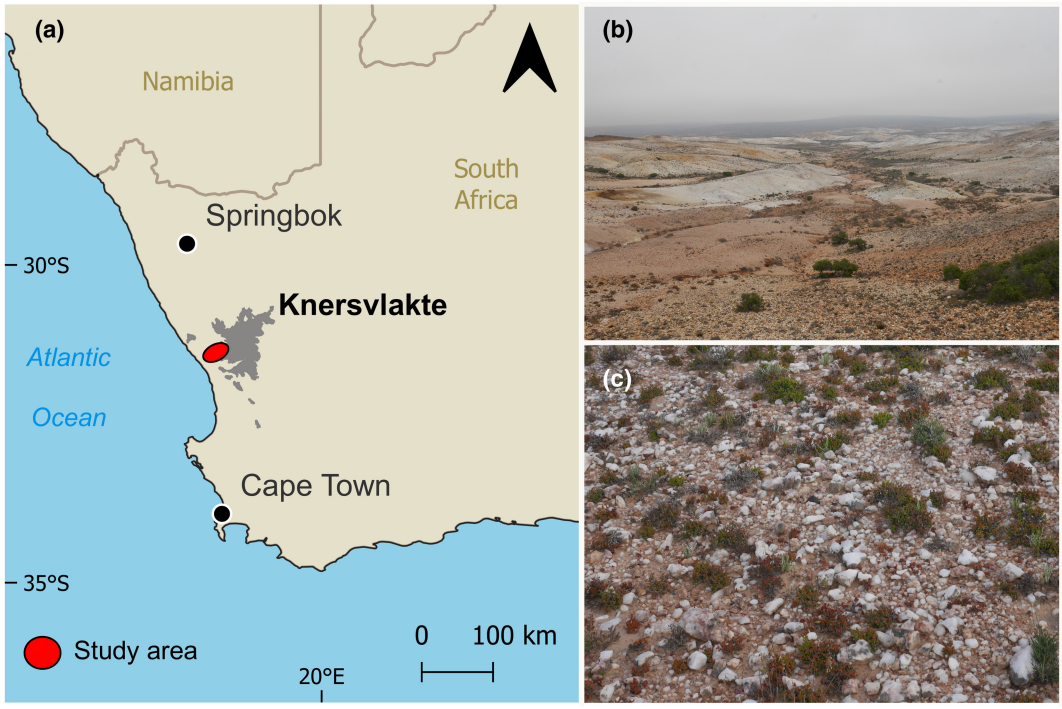

FIGURE 1 Map showing the location of the study area in the context of the Knersvlakte bioregion in South Africa (a). White quartz islands occur in this landscape on hills and in the plains (b). The ground is covered by small and large quartz pebbles and vegetation consists of small succulent shrubs (c)

2.2 | Ground truth

Ground truthing of the study area was carried out between August and October 2019. For this purpose, 47 quartz islands of various sizes and shapes were randomly selected based on image interpretation. We marked 185 locations as quartz and 67 as matrix during the ground survey. Larger islands were surveyed with multiple locations. In these cases, we kept a minimum distance of at least 150 m to ensure non-overlapping of plots at coarser image resolutions. Based on field experience we later added further expert-based training points directly in the satellite image to further refine the classification and to intensify the discrimination between different ground signals such as quartz (n = 359), matrix (n = 148), sand (n = 238), and dense vegetation (n = 156). Sand was later merged with the matrix class. In total, we assembled 1153 sampling points (i.e., quartz = 544, matrix = 453, and vegetation = 156).

2.3 | Image data

We acquired archived WorldView-2 eight-band multispectral image data (WV2) with a 2 m resolution for the study area from a commercial provider (https://www.landinfo.com). Images were taken in the dry season on April 17, 2011. Although the images were not recent, we knew that there was no landscape turnover during the last 10 years from our long-lasting field experience in the region. Image data were delivered as an orthorectified product in UTM projection (EPSG 32734) by the vendor. We further conducted an atmospheric correction using the OpticalCalibration module of the Orfeo Toolbox (McInerney & Kempeneers, 2015) to convert raw digital numbers to surface reflectance at the top of atmosphere (TOA) level. The necessary information was available in the image

metadata. As we were interested in comparing the effect of different image resolutions, we coarsened the WV2 imagery (2 m pixel size) to the different resolutions of 10 and 30 m. Resampling of satellite imagery was done in SAGA-GIS (Conrad et al., 2015) using the resampling tool and the b-spline interpolation algorithm. This had the advantage that differences in sensor and settings like acquisition time, azimuth, and spectral bandwidth did not influence our study and potential differences are expected to be merely an effect of image resolution.

As potential predictor variables we extracted all eight spectral bands (Coastal, Blue, Green, Yellow, Red, RedEdge, NIR1, NIR2) and calculated the Perpendicular Vegetation Index (PVI; Qi, Chehbouni, Huete, Kerr, & Sorooshian, 1994). The coastal and blue bands were added as we wanted to verify their potential ability to discriminate quartz signals from other reference classes. We chose the PVI over the commonly used NDVI as the performance of distance-based vegetation indices is improved for arid ecosystems (Silleos et al., 2006). Furthermore, we follow De Klerk et al. (2016) in comparing the single spectral bands (called RGB) to a dimension-reduced dataset, called PCA. We calculated the principal component analysis on the eight-band image data and retained the first three principal components (PC1, PC2, PC3).

Further, we acquired a 2 m digital elevation model (DEM) provided by the Centre for Geographical Analysis, Stellenbosch University. The data were provided in a geographic coordinate system and then projected into the same UTM system as the image data. As we were interested in how much topographical information can improve the final classification, we derived a set of topographical variables from the DEM. These were the Topographic Wetness Index (TWI), Relative Slope Height (RSH), and Total Curvature (TC). These indices are related to water availability and landscape structure, which strongly affects vegetation distribution in arid ecosystems (Abutaha, El-Khouly, Jürgens, & Oldeland, 2020; Rodríguez-Moreno & Bullock, 2014). Handling of the DEM, preparation of the topographical data, and PCA were done with SAGA-GIS (Conrad et al., 2015).

2.4 | Image segmentation

Image segmentation is the process of splitting image regions into homogeneous groups of pixels that correlate with spectral homogeneous image objects. Although commercial image segmentation packages often achieve very good results, we wanted a free and open-source solution which is applicable for small conservation management units in South Africa. We chose the seeded region-growing algorithm (Adams & Bischof, 1994) available in the toolchain "OBIA image segmentation" in SAGA-GIS (Conrad et al., 2015). This algorithm first scatters seed points across the raster dataset based on local minima and/or maxima of brightness in a channel. Then, regions are grown from the seed points until either the semi-variance signals a strong change in brightness values or when regions touch each other. The result is a polygon layer which is more or less in congruence with the spatial objects recognizable from the image data. The OBIA settings for the different resolutions were chosen after experimenting with the bandwidth parameter until a satisfying result was achieved. In general, a small bandwidth (<4) leads to small polygons, while larger values result in a reduced set of large polygons. The effect of the neighborhood and the variance in feature space was negligible, but the effect of variance in spectral space was high, so we set this parameter to 100, 60, and 20 for 2, 10, and 30 m, respectively. For each of the resulting polygon segments we calculated mean and standard deviation for each band of the four multiband raster datasets. For example, TWI_mean represents the mean of the TWI values of a single polygon while TWI_sd represents the standard deviation of all values for that particular polygon.

2.5 | Segment classification

After image segmentation, the resulting polygons have to be classified into one of the three designated land cover classes: quartz, matrix, and vegetation. We chose three different machine learning algorithms which are known

to perform well on image datasets (Liu, Abd-Elrahman, Morton, & Wilhelm, 2018; Oldeland, Revermann, Luther-Mosebach, Buttschardt, & Lehmann, 2021). These are Random Forest (RF), Artificial Neural Network (ANN), and Support Vector Machine (SVM). We refer the reader to Kuhn and Johnson (2013) for an introduction to these methods. All classification steps were carried out in the statistical programming environment R (v4.0.5; R Core Team, 2019) with the caret package (Kuhn, 2020) using the respective methods *parRF*, *nnet*, and *svmRadial*. The polygon segments were split into a training and a test dataset with an 80:20 ratio. Training the classifiers was based on a repeated 10-fold cross-validation procedure with 10 repeats. Model tuning parameters were set for each classifier individually. For RF, we incremented the number of parameters to enter at each split (mtry) from 2 to 32 (i.e., 2, 5, 8, 12, 15, 18, 22, 25, 28, 32). The number of trees was kept constant at 2000. The ANN was tuned by changing the number of nodes (size) from 1 to 10, each combined with decay values of 0.001, 0.01, and 0.1. Finally, the SVM was tuned by testing the hyperparameter "C" with values 0.25, 0.5, 1, 2, 4, 8, 16, 32, 64, and 128. Resampled data ($n = 100$) were kept with the results to allow further interpretation of training data behavior. The best training dataset was then predicted on the remaining test dataset and classifiers were evaluated.

2.6 | Model evaluation

All sets of classifier–dataset–resolution were evaluated for overall accuracy (OA), kappa (K), and F1 score (F1). While OA and kappa evaluate the classifier performance across all land cover classes, the F1 score measures the ratio of precision and recall for single classes (Kuhn & Johnson, 2013). We report F1 values only for the class of interest (i.e., "quartz islands"). Recall measures the ability of the model to find all true positives of a class in a dataset; precision measures the proportion of those predicted positive that are actually positive in the relevant class. The F1 score balances both measures as recall decreases when precision increases. For all evaluation metrics, higher values indicate a higher accuracy. Variable importance was calculated for the best-performing dataset for all resolutions and algorithms using the *varimp* function of the caret package (Kuhn, 2020). For the RF algorithm, a model-based solution to calculate variable importance is available. It is based on the comparison of the out-of-bag error for each single tree and an error after permuting the variables. For ANN and SVM, there is no model-based way to calculate importance, hence they use the area under curve (AUC) value for multiple two-class classifications (Kuhn & Johnson, 2013). For each predictor, the AUC is calculated for each pair of classes. For the target class, the maximum AUC value is identified across all pairs and used as the variable importance for that class and predictor. Thus, the importance values are not comparable between algorithms as calculations differ. Values are scaled between 0 and 100 for a better visual comparison between the resolutions.

2.7 | Effect of resolution and algorithm on island parameters

In order to better understand the effects image resolution and classification algorithms have on derived island parameters, we calculated four descriptive parameters that are commonly used in island biogeography: area, distance to nearest island, shape index, and perimeter-to-area ratio (PAR). Area and distance are important descriptive variables of islands, with area often being the most important driver of island biodiversity (MacArthur & Wilson, 1967). The shape index is used to measure shape complexity (or compactness) of an object. The interpretation of the PAR is similar in that elongated objects, or those with a complex shape, have higher ratios than objects with the same area but with a more compact shape and straight perimeter. In general, small objects usually have higher PARs than larger objects as the shape is more complex (Helzer & Jelinski, 1999). The PAR is calculated as perimeter divided by area. It is often used in conservation management to rank habitat fragments (Ciarleglio, Wesley Barnes, & Sarkar, 2009). We calculated area and distance in SAGA-GIS (Conrad et al., 2015); shape index and PAR were calculated in R using the package VLSM (Knevels, 2019).

We calculated GLMs with each island parameter as a response variable and the interaction of resolution and algorithm as fixed factors. As the parameters were highly skewed, we used the gamma family for strictly positive and skewed distributions. We checked the residuals of each model but did not find strong deviations from the assumed residual behavior (i.e., neither spatial autocorrelation nor heteroskedasticity was detected). We then used the ggeffects package (Lüdecke, 2018) to predict the marginal interaction means and confidence intervals for the specified interactions.

3 | RESULTS

3.1 | Model comparison

We applied the object-based image segmentation to 12 different image datasets. We then compared three different machine learning classifiers applied to a test dataset for OA, kappa, and F1 for the class "Quartz." In general, the PCA-based datasets were consistently ranked higher than the RGB-based datasets by the evaluation metrics (Table 1). The best-performing classifier was the ANN applied to the WorldView-2 imagery with 2 m resolution and the PCA reduced image data combined with the topographic information (Table 1). It reached the highest OA (0.88) and kappa (0.80) values, while the F1 score was slightly lower compared to the F1 score of the SVM classifier (0.912 vs. 0.916). This indicates a slightly greater accuracy at class level of the classification for the SVM. The ANN algorithm also performed best in 3 out of 4 (or 11 out of 12) datasets. In many cases SVM was the weakest classifier, while RF always performed second best.

The differences between the evaluation metrics were higher between the different resolutions than between the classifiers (Table 1, Appendix 1). In other words, the resolution had a higher impact on the classification outcome than the algorithms used for classification. The differences between the datasets were also smaller than for the different resolutions (Table 1). Very high resolution (2 m) always performed best, while the coarse resolution of Landsat 8 (30 m) performed constantly worse with OA < 0.82, kappa < 0.7, and F1 < 0.9. The resolution of

TABLE 1 Model evaluation of test datasets for the different scenarios of image resolution and data treatment

		Random forest			Artificial neural net			Support vector machine		
Dataset	**Res**	**OA**	**Kappa**	**F1**	**OA**	**Kappa**	**F1**	**OA**	**Kappa**	**F1**
PCA	2	0.825	0.705	0.877	**0.846**	**0.745**	**0.899**	**0.846**	0.741	0.885
PCA	10	0.776	0.629	0.868	0.815	0.694	0.873	0.767	0.609	0.857
PCA	30	0.752	0.584	0.824	0.770	0.605	0.860	*0.748*	*0.573*	*0.819*
PCA+TOPO	**2**	0.846	0.740	0.904	**0.880**	**0.801**	0.912	0.872	0.785	**0.916**
PCA+TOPO	10	0.845	0.742	0.909	0.853	0.759	0.913	0.845	0.741	0.903
PCA+TOPO	30	0.813	0.688	0.889	0.787	0.639	*0.869*	*0.765*	*0.604*	0.873
RGB	2	0.795	0.657	0.843	**0.859**	**0.764**	**0.896**	0.816	0.691	0.863
RGB	10	0.763	0.608	0.848	0.828	0.716	0.891	0.810	0.682	0.885
RGB	*30*	*0.752*	*0.586*	*0.831*	0.783	0.632	0.853	0.774	0.610	0.878
RGB+TOPO	2	0.842	0.735	0.900	0.863	0.771	0.896	**0.868**	**0.777**	0.900
RGB+TOPO	10	0.836	0.729	0.905	0.858	0.766	0.911	0.853	0.756	**0.912**
RGB+TOPO	30	0.778	0.630	*0.848*	0.826	0.707	0.900	*0.765*	*0.601*	0.866

Note: For each dataset, the highest values for each metric are displayed in bold while the lowest are in italics. The dataset displayed in bold was the best solution, while the dataset displayed in italics was the worst performing.
Abbreviations: OA, overall accuracy; Res, resolution.

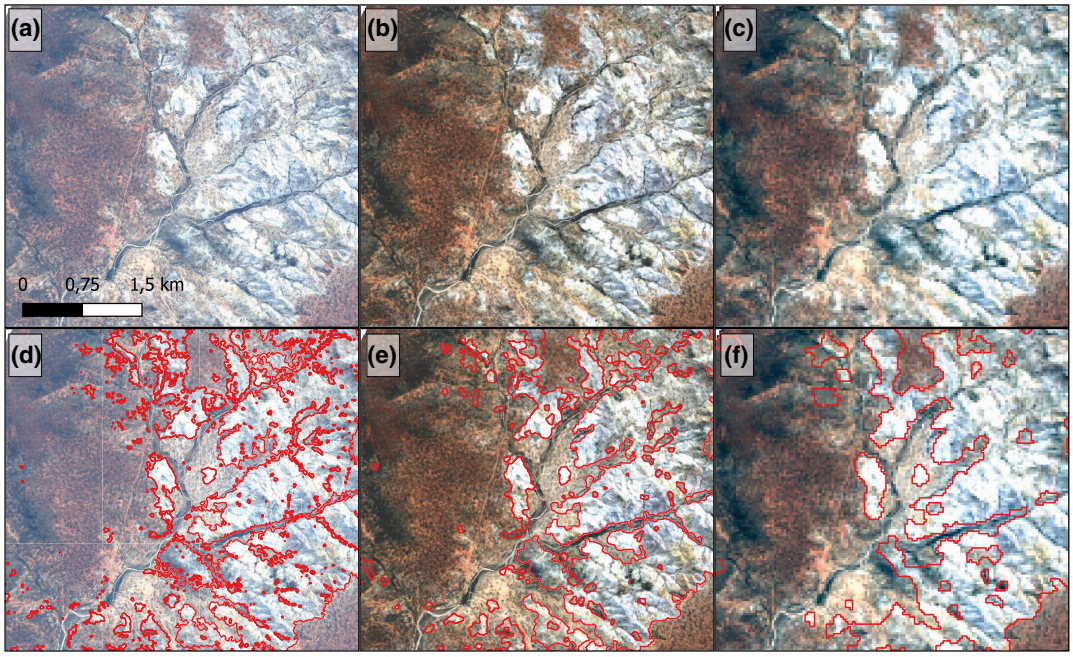

FIGURE 2 Subsets of the WorldView-2 satellite imagery on the different spatial resolutions (2 m (a + d), 10 m (b + e), 30 m (c + f)) showing white quartz islands and brown matrix vegetation. The landscape is dissected by dry riverbeds covered by dense vegetation. The lower row shows the results of the image segmentation at the respective image resolution

Sentinel 2 (10 m) was always ranked second and never performed best or worst. Depending on the algorithm, the differences between 2 and 10 m resolution were strong, with the ANN algorithm having large differences and RF the smallest differences. This makes RF a robust classifier across the range of resolutions and datasets compared, although ANN still achieves the highest accuracy. A comparison of the results for the 100 times repeated classifications of the training datasets shows that the 2 and 10 m outcomes are in some cases not significantly different (Appendix 1). Hence, both resolutions provide similar quality in terms of the evaluation criteria.

The outcome of the OBIA was displayed for the best classification model as a map overlay on the satellite imagery (Figure 2). The different maps (Figure 2a–c) show the effect of coarsening the resolution based on the same image source (i.e., WorldView-2). While the main structure remains visible in the coarsest resolution (30 m), it becomes blurry caused by the averaging of neighboring cells similar to real Landsat imagery. The differences between the 2 and 10 m resolutions seem rather subtle as even small-scale features remain visible on the 10 m scale. However, when the resulting polygon segments are compared (Figure 2d–f), it becomes apparent that there are strong differences between these resolutions. First, the number of quartz patches was five times larger on the 2 m (1002 patches) than the 10 m scale (191 patches), while on the 30 m scale only 74 patches could be determined. This discrepancy results from the much higher resolution leading to many small patches, and probably more noise. Second, all three resolutions capture the main structure of the quartz patch distribution. The coarse resolution leads to large polygons which are split into subsequent smaller polygons at the finer resolutions. None of the maps show any pattern which is not visible at a finer resolution. Hence, quartz patches themselves can be found on all scales, but the highest resolution provides most of the detail.

The variable importance for the single predictors was similar for all resolutions but differed between the algorithms (Appendix 2). The predictors PCA1_mean, PCA3_mean, and PVI_mean scored 100% for different combinations of algorithm and resolution. The topographical parameters had high and medium importance in SVM and RF, but often <50% importance for ANN. The SVM algorithm had many predictors with high importance, while

the ANN had only a few predictors with importance >50%. There were no clear differences in variable importance between mean and standard deviation values.

3.2 | Resolutions and algorithms

A map of the optimal classification model onto the WorldView-2 imagery is shown in Figure 3. It is notable that quartz islands differ from other bare soil or sandy patches, visible in the imagery, and cover about one-third of the study area (Figure 3a). The resulting landscape pattern resembles typical ocean island patterns; a large continent or main island is surrounded by many small archipelagos consisting of medium-sized or smaller islands (Figure 3b). In total, 5873 polygons and 1002 quartz islands were classified at the highest resolution, while quartz islands at 10 m ($n = 191$) and 30 m ($n = 74$) were much fewer. The statistics for the island biogeographical parameters resulting from the best-performing algorithm (ANN) differed between the three resolutions (Table 2). Median values differed strongly between the different resolutions, while maximum values differed between the algorithms by several magnitudes. For example, the maximum value for PAR at 2 m was above 0.25, while at 30 m the maximum was on average 0.05 (Figure 4). In general, at coarser resolutions the error bars become larger as there are fewer polygons.

The analysis of the categorical predictors and their interactions showed that interactions between algorithm and resolution were significant for area and PAR (Table 3). The likelihood ratios showed that resolution was always the most important factor. Still, as interactions were significant in some cases, both factors should be interpreted simultaneously when significant. By plotting the marginal means and respective confidence levels (Figure 4), several important points can be deduced. First, high-resolution imagery leads to smaller islands (i.e., smaller area values when compared to coarser resolutions). On average, the islands at 2 m resolution are several magnitudes smaller than at 10 and 30 m resolution (cf. the maps in Appendix 3). This is probably caused by delineating more

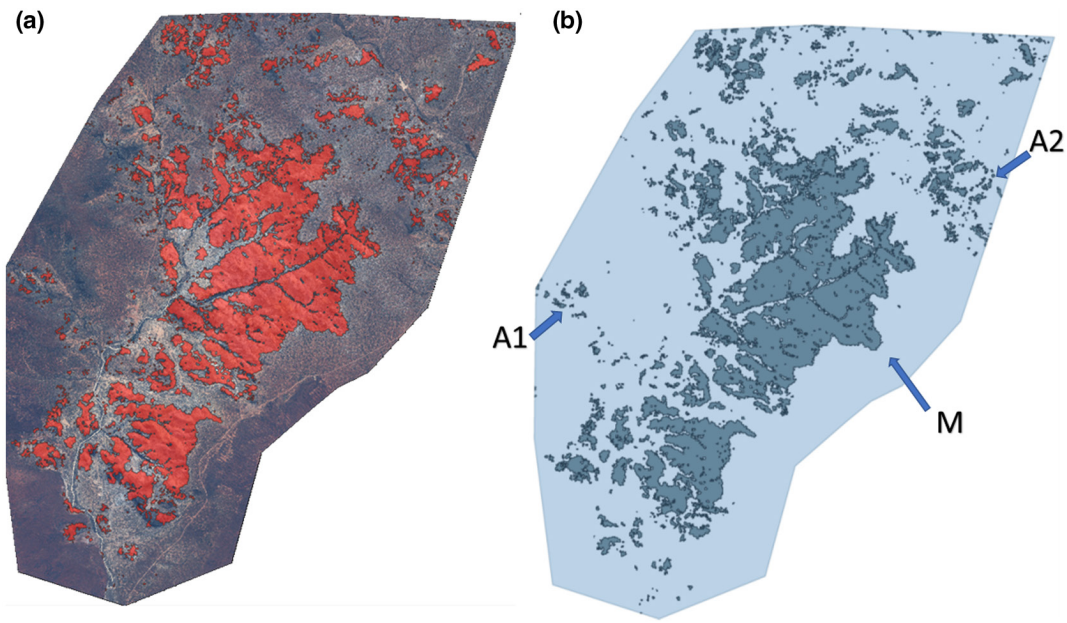

FIGURE 3 Results of the classification process overlaid on the WorldView-2 satellite image (a) and as a map (b) to highlight the island-like behavior of the quartz islands. The main island (M) is the largest contiguous quartz patch, while island clusters or archipelagos also appear at varying distances from the main island (e.g., A1, A2)

TABLE 2 Summary statistics for island biogeographical parameters based on the Artificial Neural Network (ANN) image segmentations calculated for the three different resolutions

	2 m (n = 1001)	10 m (n = 190)	30 m (n = 73)
AREA			
Mean (SD)	6870 (65,000)	35,100 (149,000)	104,000 (223,000)
Median [Min, Max]	636 [4.00, 1,950,000]	6,300 [100, 1,960,000]	39,600 [6,300, 1,700,000]
DIST			
Mean (SD)	30.5 (49.7)	91.1 (131)	161 (137)
Median [Min, Max]	16.1 [2.00, 629]	52.4 [10.0, 1,040]	120 [30.0, 720]
PAR			
Mean (SD)	0.278 (0.247)	0.0717 (0.0551)	0.0274 (0.0105)
Median [Min, Max]	0.210 [0.0214, 2.00]	0.0623 [0.0129, 0.400]	0.0258 [0.00874, 0.0571]
SHAPE			
Mean (SD)	1.74 (0.636)	1.65 (0.532)	1.63 (0.507)
Median [Min, Max]	1.53 [1.13, 8.42]	1.49 [1.13, 5.09]	1.45 [1.17, 4.22]

Note: n represents the number of quartz islands minus one, because the main island was removed from the dataset. All parameters are strongly right-skewed, hence mean and median values differ. See Appendix 4 for a complete table.

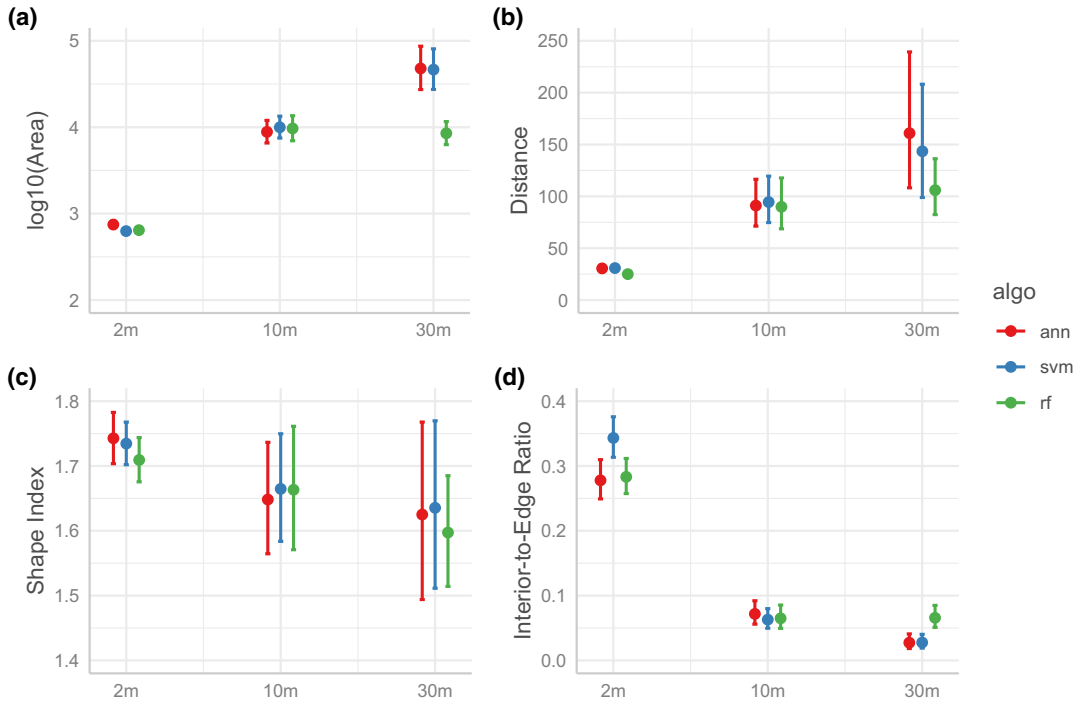

FIGURE 4 GLM results displayed as error bar plots at different spatial resolutions and algorithms. Points represent the mean and error bars the confidence interval of predicted area (a), distance (b), shape index (c), and perimeter-to-area ratio (PAR) (d). Differences are significant at the 5% level if error bars do not overlap

quartz islands at higher resolutions. Quartz islands are also more complex in shape at 2 m resolution, as indicated by the higher shape index values (Figure 4). Resolution also has a strong impact on the distance values, which are lowest for the many small islands at 2 m resolution (independent of the algorithm) and are increasingly larger at

TABLE 3 ANOVA tables (Type II) based on deviance values for the gamma GLMs

	Area			Distance			Shape			PAR		
	Chi^2	*df*	$p(Chi^2)$	Chi^2	*df*	$p(Chi^2)$	Chi^2	*df*	$p(Chi^2)$	Chi^2	*df*	$p(Chi^2)$
Res	1965.30	2	<0.001	522.10	2	<0.001	14.643	2	<0.001	433.98	2	0.064
Algo	12.92	2	<0.01	13.50	2	<0.01	1.686	2	0.430	6.45	2	<0.05
Res +Algo	42.06	4	<0.001	2.02	4	0.732	0.494	4	0.974	25.48	4	<0.001

Note: Likelihood ratio-based chi^2 values are given for the main factors of image resolution (res), classification algorithm (algo), and their interaction.

coarser resolutions. The PAR showed a mirrored pattern of area with larger (and less complex) areas having smaller PAR values. Here, differences between the algorithms are also weak (Figure 4). Furthermore, at 10 and 30 m resolution the differences are less strong, indicating less complex shapes at coarser resolutions. Statistics for all four parameters at all resolutions are listed in Appendix 4.

4 | DISCUSSION

Our study finds that the finest (2 m) resolution provided the best results for mapping the quartz island landscape in the study area of the Knersvlakte, South Africa. The moderate resolution (10 m) yielded comparable classification quality, while the coarsest resolution (30 m) was not enough to map the island patterns sufficiently. However, the optimal resolution also depends on the target size (e.g., single trees, forest patches, and single forests all require different image resolutions in order to properly capture the boundaries of the targets). Hence, the target size also influences the required image resolution. For the quartz islands of the Knersvlakte, we can confirm the outcome of the study by De Klerk et al. (2016), who compared SPOT 5 (5 m pan-sharpened to 2.5 m) versus Landsat (30 m pan-sharpened to 15 m). The higher resolutions led to more accurate classifications than the coarser resolutions. However, De Klerk et al. (2016) used two different types of sensor data and applied pan-sharpening, which distorts the spectral values, in order to improve the resolution. Thus, it is not clear how strong image processing, sensor characteristics, and different sun angles affect their results. In our approach, we have eliminated these effects by coarsening a single image. We did not apply pan-sharpening, which could have increased the resolution of the WorldView-2 imagery to 40 cm. This resolution, however, would come with a trade-off (i.e., the distortion of the spectral signals) and, depending on the pan-sharpening algorithm, not all spectral bands could have been used (Liu & Mason, 2009). Furthermore, the detail within the quartz islands could distract the algorithms from finding correct quartz island boundaries as within-object heterogeneity increases at submeter resolutions (Nagendra & Rocchini, 2008). As we did not verify the effects of pan-sharpening on our results, this additional step should be considered in future studies. Although the 2 m resolution performed best, the 10 m resolution was not significantly different. The resulting landscape pattern at 10 m contained less than half the amount of quartz islands than at 2 m and probably contained fewer tiny islands. We can conclude that very high resolution within the range of 2–10 m leads to good results in terms of model quality and credibility of the resulting quartz island pattern. We further confirm the general tendency that higher resolutions lead to better results when object-based image analysis is applied.

Our analysis showed that the ANN algorithm provided consistently good results for this particular dataset. In combination with the 2 m resolution, it provided the best performance. RF and SVM algorithms are often applied in remote sensing studies as well, and can also lead to good results (Thanh Noi & Kappas, 2018). Other studies that compared similar classification algorithms (Oldeland et al., 2021; Raczko & Zagajewski, 2017; Sothe et al., 2020) also found that ANN provides the best performance and is well suited to analyze OBIA segments. However, the performance of these machine learning classifiers often depends more on the analyzed dataset than on general

superiority. Deep learning algorithms, which were not considered here, also provided good results and should be compared in future studies (Liu et al., 2018; Sothe et al., 2020). We suggest that studies aiming at extracting and classifying image segments should always take different classification algorithms into consideration to identify the best-performing algorithm.

The interaction of image resolution and classification algorithm had a strong effect on the variability of the four island biogeographical parameters. However, there was no clear pattern in the interactions across the compared factors. In particular, the classification algorithms yielded higher and lower values without a consistent pattern. Image resolution had a stronger and much clearer effect on area and shape index. At higher resolutions, island area was smaller on average. Here, the 2 m resolution provided the smallest average island area values, while at 10 and 30 m resolution the island area was several hundred square meters larger. As the 2 m resolution is probably more accurate, coarser resolutions could significantly overestimate quartz island size. Given the high importance of area as an explanatory variable for species richness on islands (MacArthur & Wilson, 1967; Matthews, Steinbauer, Tzirkalli, Triantis, & Whittaker, 2014; Triantis, Guilhaumon, & Whittaker, 2012), the effect of image resolution should be carefully considered in future studies when extracting island patterns from image datasets, especially with respect to habitat islands.

Distance to the nearest island was also strongly affected by image resolution. Distance between islands at the 2 m resolution was significantly smaller than at coarser resolutions. This might be caused by the larger number of small or tiny islands which were rather close. At this resolution the statistical distributions of area and distance were strongly right-skewed, hence the majority of islands had only small sizes as well as small distances to the nearest island. The role of the classification algorithm is not very clear, although on the landscape scale the patterns look very different (Appendix 3). We assume that this behavior is related to stochastic elements of the classifiers and that slight changes in the imagery would lead to different outputs. In conclusion, distances depend strongly on image resolution but differ little between classification algorithms.

The shape index provided a similar picture (i.e., higher island shape complexity at the highest image resolution). Although the shape of an island should not be correlated with area per se, larger islands at the 2 m resolution were also more complex. We interpret this effect of image resolution as a matter of clearer boundary delineation. At coarser resolutions, image pixels are usually a mixture of different objects (Liu & Mason, 2009) and thus object boundaries become blurry, making it difficult to draw sharp boundaries and thus leading to long and straight edges. The fuzzy nature of many boundaries at the matrix–quartz island interface (Schmiedel et al., 2015) probably supports this effect at coarser resolutions. Hence, high resolution allows for larger and more complex islands and thus probably a more realistic pattern.

The PAR is an indicator which is used in conservation management to rank habitats (Ciarleglio et al., 2009). PAR acted like a mirrored version of the area parameter in terms of average values (i.e., lower values of PAR corresponded to higher area values, while high PAR values represented less compact but small objects that can be complex in shape). As PAR numerically depends on area, but also on shape, it behaves relatively similarly. In fact, Wang and Malanson (2007) already mention the high correlation between area and edge-related indicators. However, many island parameters used in island biogeography, and also in conservation management, depend on area. This supports our hypothesis that image resolution is an important parameter that should be discussed when island biogeographical datasets are extracted from image datasets using object-based image analysis.

High-resolution satellite imagery leads to a more precise quantification of area, distance, and shape of quartz islands. This has high relevance for nature conservation because plant species on quartz islands are often nanophytic (Schmiedel & Jürgens, 1999). Thus, their habitats are often quite small scale and their distribution very patchy. Although alpha diversity is low within each habitat, the high patchiness (habitat diversity) within an island results in high gamma diversity as a result of high beta diversity between habitats (Eibes et al., 2021). This is a likely reason why the quartz islands of the Knersvlakte are a major contributor to the exceptionally high biodiversity in the Succulent Karoo Biome (Cowling, Rundel, Desmet, & Esler, 1998). A precise quantification of area, distance,

shape, and other characteristics of quartz islands will allow conservation managers and practitioners to better balance land use and resource exploitation with the protection of these fragile and vulnerable ecosystems. Equally important, a precise quantification of quartz island characteristics enables us to apply island biogeographic theory to quartz islands to better understand the underlying processes governing taxonomic, functional, and phylogenetic diversity as well as endemism. In turn, this understanding can aid decision-making and conservation practices but can also be transferred from our model system to study other edaphic-habitat islands in dryland ecosystems worldwide (e.g., on gypsum or serpentinite).

5 | CONCLUSIONS

Four conclusions can be drawn from our study on the effects of image resolution and classification algorithms on the precision of island size and island biogeographic parameters. First, the number of islands and their sizes depend on the image resolution. Although it might be difficult to tell the "true" number of islands in a landscape, the coarser the image resolution is, the higher is the chance of missing smaller islands. High image resolution thus leads to more precision. Second, image resolution and classification algorithms showed small interaction effects. As it will be unknown beforehand if such interactions exist, we recommend explicitly checking for such interactions to better understand the model results. As expected, image resolution was important for all island-related parameters, while the shape index showed a less strong effect. Algorithms only differed at the scale of a specific resolution. Third, although the ANN had the best performance as a classifier, this may not be the case in other studies. Hence, we emphasize the need to compare multiple classification algorithms and apply hyperparameter tuning in order to get the best possible (statistical) outcome. Finally, landscape features such as the analyzed quartz islands from the Knersvlakte, an arid biodiversity hotspot of South Africa, can often be interpreted as terrestrial-habitat islands and thus island biogeographic theory can be applied, allowing theory-based conservation strategies. Future studies which aim at extracting terrestrial-habitat islands from image datasets should aim for the highest resolution and compare the outcomes of a set of different classifiers to ensure the best possible performance.

ACKNOWLEDGMENTS

We thank the CapeNature permit office for issuing research permits and the CapeNature team in Vanrhynsdorp for providing GIS shapes of the Knersvlakte Nature Reserve for the map and for their support regarding accommodation during our field work. Comments from participants of the paper-writing seminar of the working group at the University of Hamburg helped to improve an earlier version of the manuscript.

CONFLICT OF INTEREST

All authors declare that they have no conflicts of interest.

DATA AVAILABILITY STATEMENT

The data that support the findings of this study are available from the corresponding author upon reasonable request.

ORCID

Jens Oldeland https://orcid.org/0000-0002-7833-4903
Pia Maria Eibes https://orcid.org/0000-0002-6727-4204
Severin David Howard Irl https://orcid.org/0000-0002-1734-8607
Ute Schmiedel https://orcid.org/0000-0003-4059-6585

REFERENCES

Abutaha, M. M., El-Khouly, A. A., Jürgens, N., & Oldeland, J. (2020). Plant communities and their environmental drivers on an arid mountain, Gebel Elba, Egypt. *Vegetation Classification and Survey*, *1*, 21–36. https://doi.org/10.3897/VCS/2020/38644

Adams, R., & Bischof, L. (1994). Seeded region growing. *IEEE Transactions on Pattern Analysis and Machine Intelligence*, *16*, 641–647. https://doi.org/10.1109/34.295913

Burke, A. (2002). Plant communities of a Central Namib inselberg landscape. *Journal of Vegetation Science*, *13*, 483–492. https://doi.org/10.1111/j.1654-1103.2002.tb02075.x

Ciarleglio, M., Wesley Barnes, J., & Sarkar, S. (2009). ConsNet: New software for the selection of conservation area networks with spatial and multi-criteria analyses. *Ecography*, *32*(2), 205–209. https://doi.org/10.1111/j.1600-0587.2008.05721.x

Conrad, O., Bechtel, B., Bock, M., Dietrich, H., Fischer, E., Gerlitz, L., … Böhner, J. (2015). System for automated geoscientific analyses (SAGA, v. 2.1.4). *Geoscientific Model Development*, *8*, 1991–2007. https://doi.org/10.5194/gmd-8-1991-2015

Cowling, R. M., Rundel, P. W., Desmet, P. G., & Esler, K. J. (1998). Extraordinary high regional scale plant diversity in southern African arid lands: Subcontinental and global comparisons. *Diversity and Distributions*, *4*, 27–36.

Curtis, O. E., Stirton, C. H., & Muasya, A. M. (2013). A conservation and floristic assessment of poorly known species rich quartz–silcrete outcrops within Rûens Shale Renosterveld (Overberg, Western Cape), with taxonomic descriptions of five new species. *South African Journal of Botany*, *87*, 99–111. https://doi.org/10.1016/j.sajb.2013.03.017

De Klerk, H. M., Gilbertson, J., Luck-Vogel, M., Kemp, J., & Munch, Z. (2016). Using remote sensing in support of environmental management: A framework for selecting products, algorithms and methods. *Journal of Environmental Management*, *182*, 564–573. https://doi.org/10.1016/j.jenvman.2016.07.073

Desmet, P. G. (2007). Namaqualand: A brief overview of the physical and floristic environment. *Journal of Arid Environments*, *70*, 570–587. https://doi.org/10.1016/j.jaridenv.2006.11.019

Desmet, P. G., Cowling, R., Ellis, A., & Pressey, R. (2002). Integrating biosystematic data into conservation planning: Perspectives from southern Africa's Succulent Karoo. *Systematic Biology*, *51*(2), 317–330. https://doi.org/10.1080/10635150252899798

Eibes, P. M., Oldeland, J., Irl, S. D. H., Twerski, A., Kühne, N., & Schmiedel, U. (2021). Partitioned beta diversity patterns of plants across sharp and distinct boundaries of quartz habitat islands. *Journal of Vegetation Science*, *32*, e13036. https://doi.org/10.1111/jvs.13036

Ellis, A. G., & Weis, A. E. (2006). Coexistence and differentiation of 'flowering stones': The role of local adaptation to soil microenvironment. *Journal of Ecology*, *94*, 322–335. https://doi.org/10.1111/j.1365-2745.2005.01074.x

Ellis, A. G., Weis, A. E., & Gaut, B. S. (2006). Evolutionary radiation of "stone plants" in the genus *Argyroderma* (Aizoaceae): Unraveling the effects of landscape, habitat, and flowering time. *Evolution*, *60*, 39–55. https://doi.org/10.1111/j.0014-3820.2006.tb01080.x

Helzer, C. J., & Jelinski, D. E. (1999). The relative importance of patch area and perimeter–area ratio to grassland breeding birds. *Ecological Applications*, *9*(4), 1448–1458. https://doi.org/10.2307/2641409

Hoffman, T., Skowno, A., Bell, W., & Mashele, S. (2018). Long-term changes in land use, land cover and vegetation in the Karoo drylands of South Africa: Implications for degradation monitoring. *African Journal of Range & Forage Science*, *35*, 209–221. https://doi.org/10.2989/10220119.2018.1516237

Itescu, Y. (2019). Are island-like systems biologically similar to islands? A review of the evidence. *Ecography*, *42*, 1298–1314. https://doi.org/10.1111/ecog.03951

Kier, G., Kreft, H., Lee, T. M., Jetz, W., Ibisch, P. L., Nowicki, C., … Barthlott, W. (2009). A global assessment of endemism and species richness across island and mainland regions. *Proceedings of the National Academy of Sciences of the United States of America*, *106*, 9322–9327. https://doi.org/10.1073/pnas.0810306106

Knevels, R. (2019). *VLSM: Vector-based landscape metrics* (R package version 0.0.0-9002). Retrieved from https://github.com/raff-k/VLSM

Kuhn, M. (2020). *caret: Classification and regression training* (R package version 6.0-86). Retrieved from https://CRAN.R-project.org/package=caret

Kuhn, M., & Johnson, K. (2013). *Applied predictive modeling*. New York, NY: Springer.

Liu, J.-G., & Mason, P. J. (2009). *Essential image processing and GIS for remote sensing*. Chichester, UK: Wiley-Blackwell.

Liu, T., Abd-Elrahman, A., Morton, J., & Wilhelm, V. L. (2018). Comparing fully convolutional networks, random forest, support vector machine, and patch-based deep convolutional neural networks for object-based wetland mapping using images from small unmanned aircraft system. *Giscience & Remote Sensing*, *55*, 243–264. https://doi.org/10.1080/15481603.2018.1426091

Lüdecke, D. (2018). ggeffects: Tidy data frames of marginal effects from regression models. *Journal of Open Source Software*, *3*, 772. https://doi.org/10.21105/joss.00772

MacArthur, R. H., & Wilson, E. O. (1967). *The theory of island biogeography*. Princeton, NJ: Princeton University Press.

Matthews, T. J. (2021). On the biogeography of habitat islands: The importance of matrix effects, noncore species, and source–sink dynamics. *The Quarterly Review of Biology*, *96*, 73–104. https://doi.org/10.1086/714482

Matthews, T. J., Steinbauer, M. J., Tzirkalli, E., Triantis, K. A., & Whittaker, R. J. (2014). Thresholds and the species–area relationship: A synthetic analysis of habitat island datasets. *Journal of Biogeography*, *41*, 1018–1028. https://doi.org/10.1111/jbi.12286

McInerney, D., & Kempeneers, P. (2015). *Open source geospatial tools: Earth systems data and models* (Orfeo toolbox, pp. 199–217). Cham, Switzerland: Springer. https://doi.org/10.1007/978-3-319-01824-9_13

Mendez-Castro, F. E., Conti, L., Chytrý, M., Jiménez-Alfaro, B., Hájek, M., Horsák, M., … Ottaviani, G. (2021). What defines insularity for plants in edaphic islands? *Ecography*, *44*(8), 1249–1258. https://doi.org/10.1111/ecog.05650

Mucina, L., Jürgens, N., Le Roux, A., Rutherford, M. C., Schmiedel, U., Esler, K. J., … Milton, S. J. (2006). Succulent Karoo biome. In L. Mucina & M. C. Rutherford (Eds.), *The vegetation of South Africa, Lesotho and Swaziland* (pp. 221–229). Pretoria, South Africa: South African National Biodiversity Institute.

Nagendra, H., & Rocchini, D. (2008). High resolution satellite imagery for tropical biodiversity 630 studies: The devil is in the detail. *Biodiversity and Conservation*, *17*, 3431–3442. https://doi.org/10.1007/s10531-008-9479-0

Oldeland, J., Revermann, R., Luther-Mosebach, J., Buttschardt, T., & Lehmann, J. R. K. (2021). New tools for old problems: Comparing drone- and field-based assessments of a problematic plant species. *Environmental Monitoring and Assessment*, *193*, 90. https://doi.org/10.1007/s10661-021-08852-2

Ottaviani, G., Keppel, G., Götzenberger, L., Harrison, S., Opedal, Ø. H., Conti, L., … Chytrý, M. (2020). Linking plant functional ecology to island biogeography. *Trends in Plant Science*, *25*, 329–339. https://doi.org/10.1016/j.tplants.2019.12.022

Qi, J., Chehbouni, A., Huete, A. R., Kerr, Y. H., & Sorooshian, S. (1994). A modified soil adjusted vegetation index. *Remote Sensing of Environment*, *48*, 119–126. https://doi.org/10.1016/0034-4257(94)90134-1

R Core Team. (2019). *R: A language and environment for statistical computing*. Vienna, Austria: R Foundation for Statistical Computing. https://www.r-project.org

Raczko, E., & Zagajewski, B. (2017). Comparison of support vector machine, random forest and neural network classifiers for tree species classification on airborne hyperspectral APEX images. *European Journal of Remote Sensing*, *50*, 144–154. https://doi.org/10.1080/22797254.2017.1299557

Rocchini, D., Petras, V., Petrasova, A., Horning, N., Furtkevicova, L., Neteler, M., … Wegmann, M. (2017). Open data and open source for remote sensing training in ecology. *Ecological Informatics*, *40*, 57–61. https://doi.org/10.1016/j.ecoinf.2017.05.004

Rodríguez-Caballero, E., Paul, M., Tamm, A., Caesar, J., Büdel, B., Escribano, P., … Weber, B. (2017). Biomass assessment of microbial surface communities by means of hyperspectral remote sensing data. *Science of the Total Environment*, *586*, 1287–1297. https://doi.org/10.1016/j.scitotenv.2017.02.141

Rodríguez-Moreno, V. M., & Bullock, S. H. (2014). Vegetation response to hydrologic and geomorphic factors in an arid region of the Baja California Peninsula. *Environmental Monitoring and Assessment*, *186*, 1009–1021. https://doi.org/10.1007/s10661-013-3435-5

Schmiedel, U. (2002). *The quartz fields of southern Africa. Flora, phytogeography, vegetation, and habitat ecology* (Unpublished PhD dissertation). Cologne, Germany: University of Cologne.

Schmiedel, U. (2004). The phytogeography of the obligate quartz field flora of southern Africa. *Schumannia*, *4*, 181205.

Schmiedel, U., & Jürgens, N. (1999). Community structure on unusual habitat islands: Quartz fields in the Succulent Karoo, South Africa. *Plant Ecology*, *142*, 57–69. https://doi.org/10.1023/A:1009818210799

Schmiedel, U., Kühne, N., Twerski, A., & Oldeland, J. (2015). Small-scale soil patterns drive sharp boundaries between succulent "dwarf" biomes (or habitats) in the arid Succulent Karoo, South Africa. *South African Journal of Botany*, *101*, 129–138. https://doi.org/10.1016/j.sajb.2015.05.001

Silleos, N. G., Alexandridis, T. K., Gitas, I. Z., & Perakis, K. (2006). Vegetation indices: Advances made in biomass estimation and vegetation monitoring in the last 30 years. *Geocarto International*, *21*(4), 21–28. https://doi.org/10.1080/10106040608542399

Sothe, C., De Almeida, C. M., Schimalski, M. B., La Rosa, L. E. C., Castro, J. D. B., Feitosa, R. Q., … Tommaselli, A. M. G. (2020). Comparative performance of convolutional neural network, weighted and conventional support vector machine and random forest for classifying tree species using hyperspectral and photogrammetric data. *Giscience & Remote Sensing*, *57*, 369–394. https://doi.org/10.1080/15481603.2020.1712102

Thanh Noi, P., & Kappas, M. (2018). Comparison of Random Forest, k-Nearest Neighbor, and Support Vector Machine classifiers for land cover classification using Sentinel-2 imagery. *Sensors*, *18*, 18. https://doi.org/10.3390/s18010018

Triantis, K. A., Guilhaumon, F., & Whittaker, R. J. (2012). The island species–area relationship: Biology and statistics. *Journal of Biogeography*, *39*, 215–231. https://doi.org/10.1111/j.1365-2699.2011.02652.x

Van Tonder, C., Milton, S. J., & Cameron, M. J. (2014). Livestock paths on Namaqualand quartz fields: Will the endemic flora disappear? *South African Journal of Botany*, *95*, 19–23. https://doi.org/10.1016/j.sajb.2014.07.014

Wang, Q., & Malanson, G. P. (2007). Patterns of correlation among landscape metrics. *Physical Geography*, *28*, 170–182. https://doi.org/10.2747/0272-3646.28.2.170

Watkeys, M. K. (1999). Soils of the arid south-western zone of Africa. In W. R. J. Dean & S. J. Milton (Eds.), *The Karoo: Ecological patterns and processes* (pp. 17–25). Cambridge, UK: Cambridge University Press.

Wintle, B. A., Kujala, H., Whitehead, A., Cameron, A., Veloz, S., Kukkala, A., … Bekessy, S. A. (2019). Global synthesis of conservation studies reveals the importance of small habitat patches for biodiversity. *Proceedings of the National Academy of Sciences of the United States of America*, *116*(3), 909–914. https://doi.org/10.1073/pnas.1813051115

How to cite this article: Oldeland, J., Eibes, P. M., Irl, S. D. H., & Schmiedel, U. (2022). Do image resolution and classifier choice impact island biogeographical parameters of terrestrial islands? *Transactions in GIS*, *26*, 2004–2022. https://doi.org/10.1111/tgis.12920

APPENDIX 1

Model evaluation for resampled training data. Each resampling consists of 100 repetitions based on 10 cross-validation runs each with 10 repeats. Overall Accuracy (a) and Kappa (b) led to the same ordering

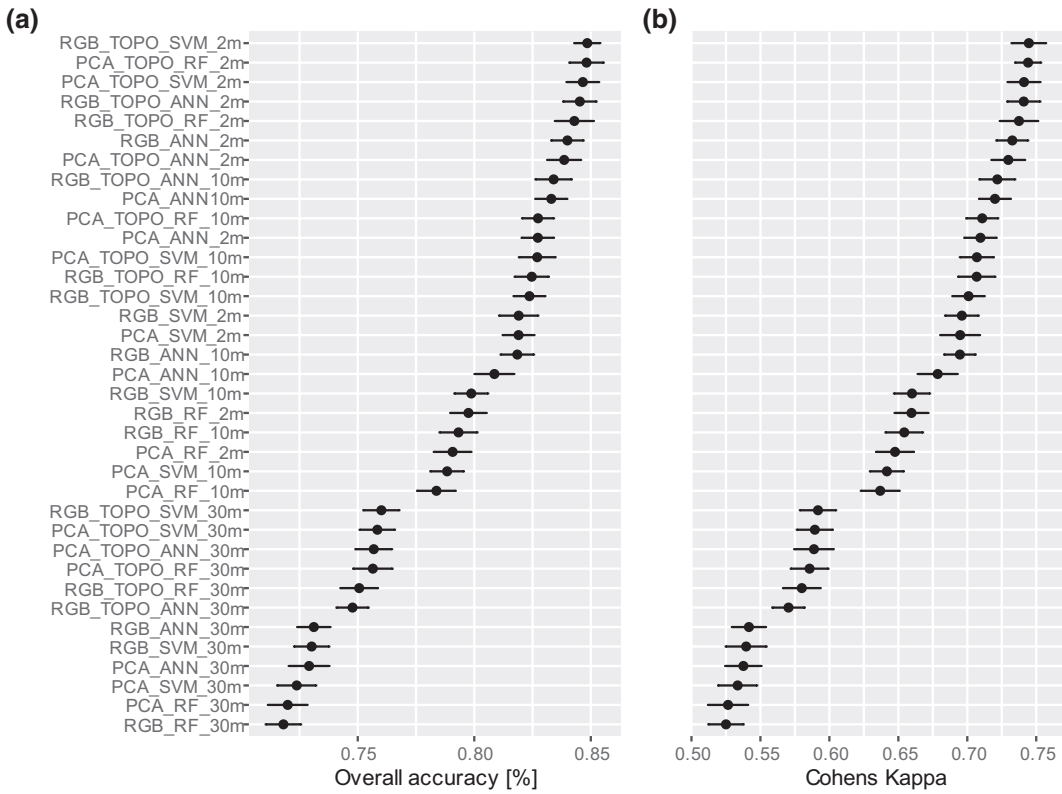

APPENDIX 2

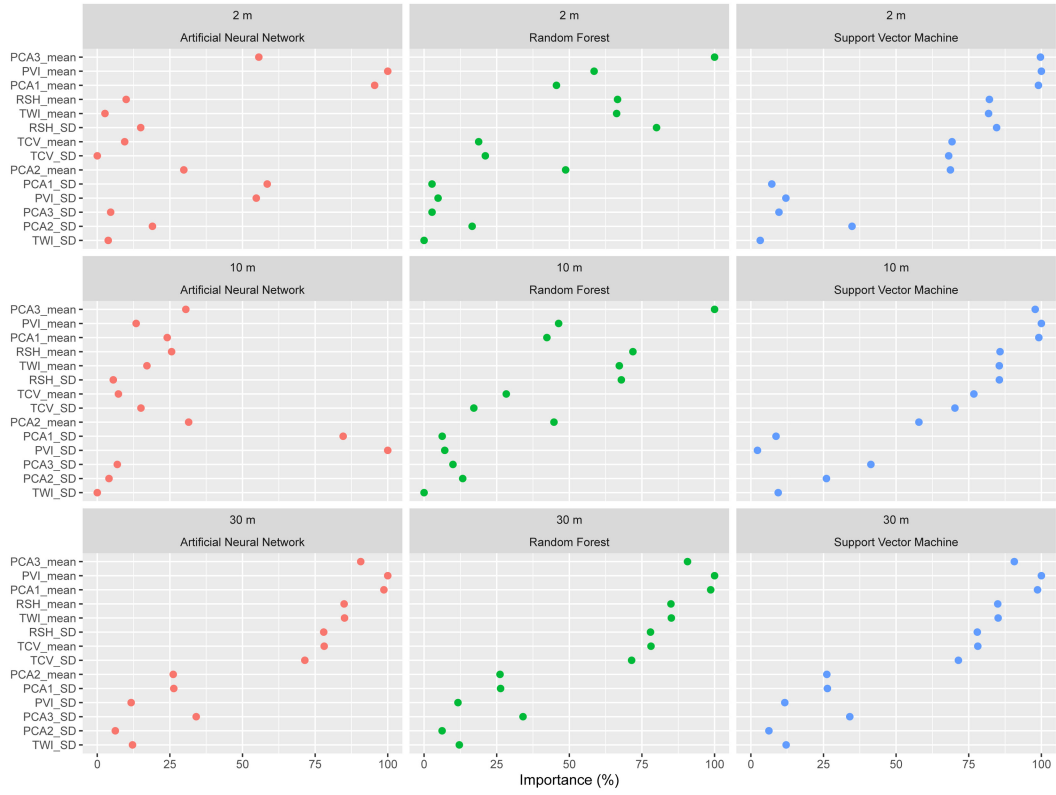

NOTE: Variable importance ist not comparable between model types

APPENDIX 3

QUARTZ ISLANDS DATASETS

Image source World-View 2 m (PCA + TOPO)
Image segmentation based on seeded region growing
Classification done with Artificial Neural Network
CRS: UTM 34S / WGS 84

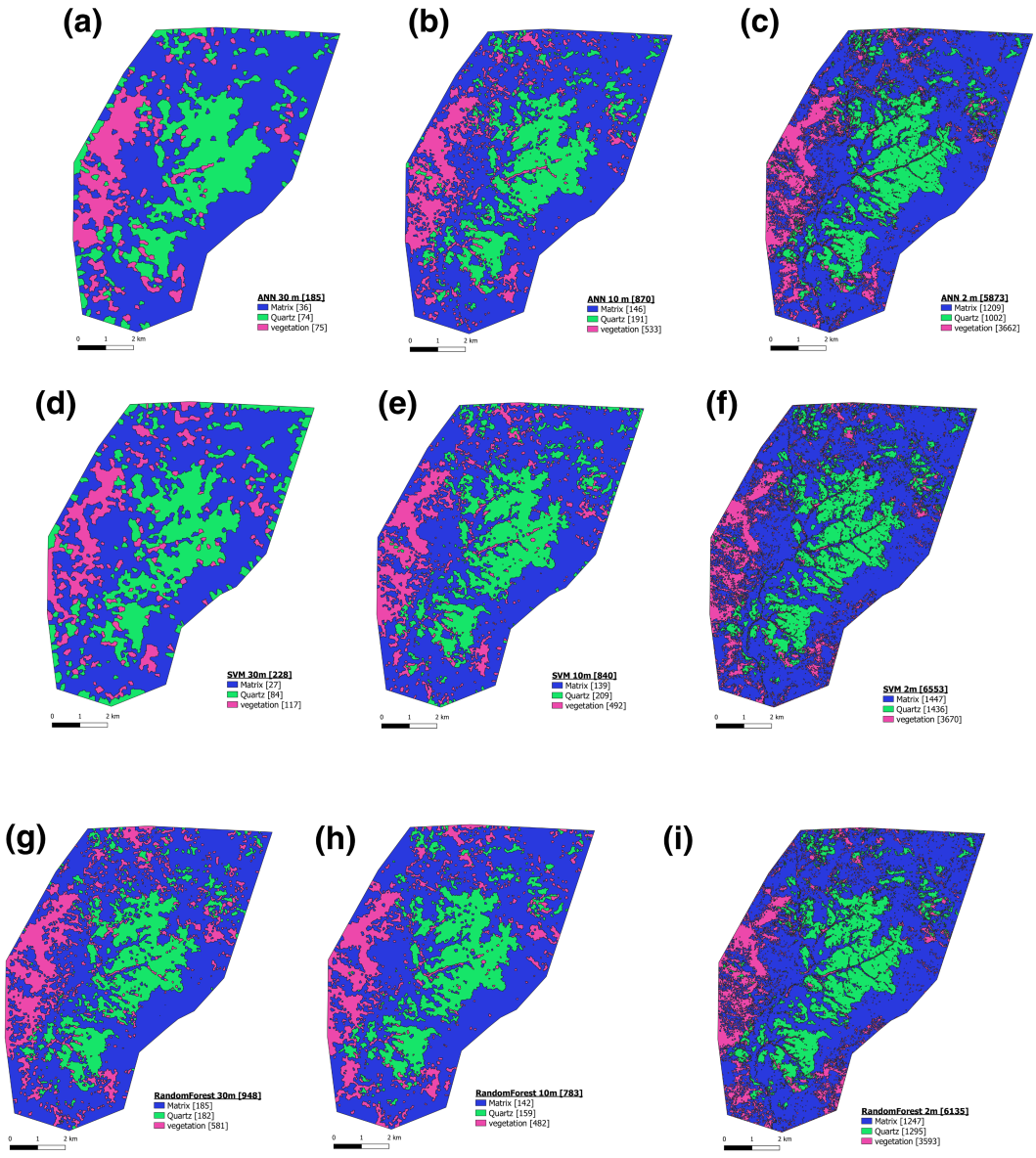

APPENDIX 4

	2 m			10 m			30 m		
	ann (*N* = 1001)	rf (*N* = 1294)	svm (*N* = 1435)	ann (*N* = 190)	rf (*N* = 158)	svm (*N* = 208)	ann (*N* = 73)	rf (*N* = 181)	svm (*N* = 83)
AREA									
Mean (SD)	6870 (65,000)	5880 (47,300)	5220 (53,800)	35,100 (149,000)	36,500 (129,000)	32,100 (142,000)	104,000 (223,000)	30,600 (178,000)	82,900 (127,000)
Median [Min, Max]	636 [4.00, 1,950,000]	530 [4.00, 1,440,000]	544 [0.0242, 1,900,000]	6300 [100, 1,960,000]	6400 [600, 1,480,000]	7150 [600, 1,990,000]	39,600 [6300, 1,700,000]	6600 [200, 2,380,000]	36,900 [6300, 828,000]
DIST									
Mean (SD)	30.5 (49.7)	25.0 (42.7)	30.9 (61.9)	91.1 (131)	89.9 (100)	94.5 (137)	161 (137)	106 (175)	143 (122)
Median [Min, Max]	16.1 [2.00, 629]	14.0 [2.00, 543]	16.1 [1.47, 984]	52.4 [10.0, 1040]	50.0 [10.0, 579]	53.6 [10.0, 1070]	120 [30.0, 720]	51.0 [10.0, 1160]	108 [30.0, 708]
IER									
Mean (SD)	0.278 (0.247)	0.283 (0.227)	0.343 (1.01)	0.0717 (0.0551)	0.0650 (0.0305)	0.0630 (0.0280)	0.0274 (0.0105)	0.0658 (0.0329)	0.0276 (0.00981)
Median [Min, Max]	0.210 [0.0214, 2.00]	0.228 [0.0191, 2.00]	0.226 [0.0226, 32.9]	0.0623 [0.0129, 0.400]	0.0625 [0.0113, 0.167]	0.0592 [0.0128, 0.167]	0.0258 [0.00874, 0.0571]	0.0623 [0.0134, 0.300]	0.0261 [0.0115, 0.0571]
SHAPE									
Mean (SD)	1.74 (0.636)	1.71 (0.629)	1.73 (0.685)	1.65 (0.532)	1.66 (0.521)	1.66 (0.516)	1.63 (0.507)	1.60 (0.519)	1.64 (0.521)
Median [Min, Max]	1.53 [1.13, 8.42]	1.51 [1.13, 7.36]	1.52 [1.13, 8.78]	1.49 [1.13, 5.09]	1.48 [1.15, 3.96]	1.49 [1.15, 5.09]	1.45 [1.17, 4.22]	1.43 [1.18, 5.85]	1.49 [1.16, 4.48]